PROTEINS
STRUCTURE ■ FUNCTION ■ BIOINFORMATICS

STRUCTURE NOTE

Atomic structure of the nuclear pore complex targeting domain of a Nup116 homologue from the yeast, *Candida glabrata*

Parthasarathy Sampathkumar,[1,2*] Seung Joong Kim,[3,4,5] Danalyn Manglicmot,[2] Kevin T. Bain,[2] Jeremiah Gilmore,[2] Tarun Gheyi,[2] Jeremy Phillips,[3,4,5,6] Ursula Pieper,[3,4,5] Javier Fernandez-Martinez,[7] Josef D. Franke,[7] Tsutomu Matsui,[8] Hiro Tsuruta,[8,†] Shane Atwell,[2] Devon A. Thompson,[2] J. Spencer Emtage,[2] Stephen R. Wasserman,[9] Michael P. Rout,[7] Andrej Sali,[3,4,5] J. Michael Sauder,[2] Steven C. Almo,[1] and Stephen K. Burley[2]

[1] Department of Biochemistry, Albert Einstein College of Medicine, Bronx, New York 10461

[2] Translational Sciences and Technology (TS&T), Eli Lilly and Company, Lilly Biotechnology Center, San Diego, California 92121

[3] Department of Bioengineering and Therapeutic Sciences, University of California, San Francisco, California 94158

[4] Department of Pharmaceutical Chemistry, University of California, San Francisco, California 94158

[5] California Institute for Quantitative Biosciences, University of California, San Francisco, California 94158

[6] Graduate Group in Biological and Medical Informatics, University of California, San Francisco, California 94158

[7] Laboratory of Cellular and Structural Biology, The Rockefeller University, New York 10065

[8] Stanford Synchrotron Radiation Lightsource, SLAC National Accelerator Laboratory, Stanford University, Menlo Park, California 94025

[9] LRL-CAT, Eli Lilly and Company, Advanced Photon Source, Argonne National Laboratory, Argonne, Illinois 60439

ABSTRACT

The nuclear pore complex (NPC), embedded in the nuclear envelope, is a large, dynamic molecular assembly that facilitates exchange of macromolecules between the nucleus and the cytoplasm. The yeast NPC is an eightfold symmetric annular structure composed of ~456 polypeptide chains contributed by ~30 distinct proteins termed nucleoporins. Nup116, identified only in fungi, plays a central role in both protein import and mRNA export through the NPC. Nup116 is a modular protein with N-terminal "FG" repeats containing a Gle2p-binding sequence motif and a NPC targeting domain at its C-terminus. We report the crystal structure of the NPC targeting domain of *Candida glabrata* Nup116, consisting of residues 882–1034 [CgNup116(882–1034)], at 1.94 Å resolution. The X-ray structure of CgNup116(882–1034) is consistent with the molecular envelope determined in solution by small-angle X-ray scattering. Structural similarities of CgNup116(882–1034) with homologous domains from *Saccharomyces cerevisiae* Nup116, *S. cerevisiae* Nup145N, and human Nup98 are discussed.

Proteins 2012; 80:2110–2116.

Key words: nuclear pore complex; Nup116; Nup98; Nup100; Nup145; mRNA export; structural genomics.

Additional Supporting Information may be found in the online version of this article.

[†]Deceased on August 25, 2011

Grant sponsors: NIH Grants U01 GM098256, U54 GM074945, U54 GM094662, NIH R01 GM062427 (MPR), NIH R01 GM083960, NIH U54 RR022220, The US Department of Energy, Office of Basic Energy Sciences, the DOE Office of Biological and Environmental Research; Grant sponsor: The National Institutes of Health, National Center for Research Resources, Biomedical Technology Program; Grant number: P41RR001209.

*Correspondence to: Parthasarathy Sampathkumar, Department of Biochemistry, Albert Einstein College of Medicine, Ullmann Building, Room 409, 1300 Morris Park Avenue, Bronx, NY 10461. E-mail: psampath@aecom.yu.edu

Received 27 January 2012; Revised 5 April 2012; Accepted 11 April 2012
Published online 27 April 2012 in Wiley Online Library (wileyonlinelibrary.com). DOI: 10.1002/prot.24102

INTRODUCTION

Transport of macromolecules between nucleus and cytoplasm is an essential eukaryotic process facilitated by the nuclear pore complex (NPC). In addition to its role in normal physiology, NPC loss of function has been implicated in cancer and autoimmune disease.[1,2] In yeast (e.g., *Saccharomyces*), NPCs are large, eightfold symmetric dynamic macromolecular assemblies composed of at least 456 polypeptide chains derived from multiple copies of ~30 distinct nucleoporins (Nups).[3,4] Several of these components share similar structural motifs and form stable subcomplexes that contribute to the overall organization of the assembly, which includes two outer rings (the nuclear and cytoplasmic rings), two inner rings, and a membrane-associated ring.[5,6]

Nup116,[7] a Nup identified only in fungi, is involved in both protein import and mRNA export.[8] Nup116 shows an asymmetric radial distribution within the NPC, with a bias toward the cytoplasmic face.[9] Nup116 is homologous to yeast Nup100; it is also homologous to yeast Nup145N and human Nup98, both of which are derived from a larger precursor by autoproteolysis.[10,11] Nup116 is a modular protein with N-terminal "FG" repeats and a C-terminal domain, supporting NPC localization.[12] The "FG" repeats are thought to transiently interact with nuclear transport factors to ensure the transport of specific proteins and ribonucleoprotein complexes.[13] A distinguishing feature of Nup116, when compared to both Nup100 and Nup145N, is the presence of an N-terminal Gle2p-binding[14] sequence (GLEBS, ~60 amino acid residue motif), responsible for targeting the RNA export factor Rae1/Gle2p to the NPC. A GLEBS motif is also present in human Nup98.[15] The crystal structure of a human Rae1:Nup98-GLEBS domain complex revealed that GLEBS contains a hairpin motif required for the interaction with Rae1.[16]

Although the N-terminal domain of Nup116 mediates interactions with nuclear transport factors, its C-terminal domain (referred to as NPC targeting domain) localizes Nup116 to the NPC and plays an essential role in NPC assembly. The NPC targeting domain of Nup116 interacts directly with the Nup82–Nsp1–Nup159 complex.[12] Herein, we report the 1.94 Å resolution crystal structure of the NPC targeting domain of *C. glabrata* Nup116 (residues, 882–1034; CgNup116[882–1034]) and the results of complementary solution studies using small-angle X-ray scattering (SAXS). We also present detailed structural comparisons with the previously reported structures of *Saccharomyces cerevisiae* Nup116 (ScNup116; residues, 967–1113; apo form determined by NMR spectroscopy[17] and the heterotrimer with Nup82:Nup159 complex determined by X-ray crystallography[18]), Nup145N (ScNup145N; residues, 443–605 X-ray[19]), and human Nup98 (HsNup198; residues, 716–870; X-ray[10,11]).

MATERIALS AND METHODS

Cloning, expression, and purification of CgNup116(882–1034)

The gene encoding Nup116 from *C. glabrata* was cloned from genomic DNA of strain 2001D-5_CBS 138 (American Type Culture Collection, USA). The desired truncation (encoding residues, 882–1034) was PCR amplified using GATGGCATTGATGATCTAGAATTTG and CTAATGCATGATCAACAGTGAAGCAG as forward and reverse primers, respectively. The purified PCR product was TOPO® (Invitrogen, USA) cloned into pSGX3, a derivative of pET26b(+), yielding a protein with a noncleavable C-terminal hexahistidine tag. The resulting plasmid was transformed into BL21(DE3)-Condon+RIL (Invitrogen, USA) cells for expression. Production of Se-Met protein[20] was carried out in 1 L of HY media at 22°C containing 50 μg/mL of kanamycin and 35 μg/mL of chloramphenicol. Protein expression was induced by addition of 0.4 m*M* IPTG. Cells were harvested after 21 h by centrifugation at 4°C.

For purification, the *Escherichia coli* cell pellet was resuspended in 30 mL of cold buffer containing 20 m*M* Tris–HCl, pH 8.0, 500 m*M* NaCl, 25 m*M* imidazole, and 0.1% (v/v) Tween-20 and the cells were lysed by sonication. Cell debris was removed by centrifugation at 4°C. The supernatant was applied to a 5-mL HisTrapHP column (GE Healthcare, USA) charged with nickel and pre-equilibrated with 20 m*M* Tris–HCl, pH 8.0, 500 m*M* NaCl, 10% (v/v) glycerol, and 25 m*M* imidazole. The sample was washed with five column volumes (CVs) of 20 m*M* Tris–HCl, pH 8.0, 500 m*M* NaCl, 10% (v/v) glycerol, and 40 m*M* imidazole, and subsequently eluted with 2 CV of same buffer with an imidazole concentration of 250 m*M*. Eluted protein was further purified over a 120 mL Superdex 200 size exclusion column equilibrated with 10 m*M* HEPES, pH 7.5, 150 m*M* NaCl, 10% (v/v) glycerol, and 5 m*M* dithiothreitol (protein storage buffer). SDS-PAGE analysis demonstrated >95% purity. Protein fractions corresponding to the central portion of the size exclusion chromatography profile were pooled, concentrated by AMICON spin filtration, and aliquots were frozen in liquid nitrogen and stored at −80°C.

Crystallization, data collection, and structure determination

Initial crystals of CgNup116(882–1034) were obtained in several PEG-containing conditions *via* sitting drop vapor diffusion at 21°C (~10.4 mg/mL; 0.3 μL protein + 0.3 μL reservoir solution). Subsequent optimization was carried out with an additive screen (Hampton Research, USA) and macroseeding. Diffraction quality crystals were obtained with 100 m*M* MES, pH 6.2, 25% (w/v) PEG MME 2K, and 200 m*M* sodium potassium tartrate. The

Table I
Crystallographic Statistics

Data collection	CgNup116(883–1034)
PDB code	3NF5
Space group	$P2_1$
Unit-cell dimensions (Å)	$a = 48.7$, $b = 67.7$, $c = 55.1$, $\beta = 101.4^\circ$
Matthew's coefficient (Å^3/Da)	2.38
Solvent content (%)	48
Resolution (Å)	34.37–1.94 (2.04–1.94)[a]
Number of unique reflections	25,957 (3756)
Completeness (%)	99.1 (98.8)
R_{symm} (%)	14.0 (47.1)
Multiplicity	7.0 (6.9)
$<I/\sigma(I)>$	8.3 (3.6)
Refinement	
R-factor (%)	20.7
R_{free} (%)	25.6
r.m.s.d.s from ideal values	
Bond length (Å)	0.020
Bond angles (°)	1.782
Ramachandran Plot[42]	
MolProbity[43] *residues in*	
Favored region (%)	97.0
Allowed region (%)	100.0

[a]Values in parenthesis correspond to the highest resolution shell.

final sitting drops contained 1.0 μL of CgNup116(882–1034) at 10.85 mg/mL, 0.6 μL of reservoir solution, and 0.4 μL of 5% (v/v) ethyl acetate from the additive screen. Crystals were cryoprotected by addition of glycerol (final concentration, ~30% (v/v)) and flash cooled by immersion in liquid nitrogen. Diffraction data were recorded at the LRL-CAT 31-ID beamline (Advanced Photon Source [APS]) and processed with MOSFLM[21] and SCALA (CCP4).[22] Structure was determined by molecular replacement using PHASER[23] with a polyalanine model of ScNup145N (PDB Code 3KEP).[19] Initial model building was carried out with ARP/wARP,[24] followed by manual rebuilding with COOT.[25] The atomic model of CgNup116(882–1034) was refined to convergence using REFMAC5[26] and exhibited excellent stereochemistry (Table I). Illustrations were prepared with PyMol.[27]

Small-angle X-ray scattering

SAXS measurements of CgNup116(882–1034) were carried out at Beamline 4-2 of the Stanford Synchrotron Radiation Lightsource. The beam energy and current were 11 keV and 200 mA, respectively. A silver behenate sample was used to calibrate the q-range and detector distance. Data collection was controlled with Blu-Ice.[28] We used an automatic sample delivery system equipped with a 1.5 mm-diameter thin-wall quartz capillary within which a sample aliquot was oscillated in the X-ray beam to minimize radiation damage. The sample was placed at 1.7 m from a Rayonix MX225-HE (MAR-USA, USA) CCD detector with a binned pixel size of 293 μm × 293 μm. Ten 3-s exposures were made for each of the four protein samples maintained at 15°C. Each of the 10 diffraction images was scaled by the transmitted beam intensity, using SASTool (http://ssrl.slac.stanford.edu/~saxs/analysis/sastool.htm, formerly MarParse), and averaged to obtain fully processed data in the form of intensity versus q ($q = 4\pi\sin(\theta)/\lambda$, where θ is one-half of the scattering angle and λ is the X-ray wavelength). The buffer SAXS profile was obtained in the same manner and subtracted from a protein profile. SAXS profiles of CgNup116(882–1034) were recorded at protein concentrations of 0.5, 1.0, 2.0, and 5.0 mg/mL in the protein storage buffer. Mild concentration dependence of the profiles was eliminated by extrapolating to zero concentration. The average of the lower scattering angle parts ($q < 0.15$ Å^{-1}) of the lower concentration profiles (0.5–1.0 mg/mL) and the average of the higher scattering angle parts ($q > 0.12$ Å^{-1}) of the higher concentration (1.5–5.0 mg/mL) profiles were merged to obtain the final experimental SAXS profile. The merged experimental SAXS profile was compared with SAXS profiles calculated for the monomer (Chain A) and for the crystallographic asymmetric unit (Chains A and B) of CgNup116(882–1034) with IMP FoXS (http://salilab.org/foxs).[29,30] A complete monomer model of CgNup116(882–1034), which included a C-terminal hexahistidine tag (Gly-His-His-His-His-His-His), eight side chains not modeled in the crystal structure, and two Se-Met residues, was generated using the crystal structure with the automodel function of MODELLER[31] and customized scripts in IMP.[32] Inclusion of the missing atoms further improved the fit of the calculated and experimental profiles (χ-value improved from 1.33 to 1.11). The shape of CgNup116(882–1034) was calculated from the merged experimental SAXS profile by running DAMMIF[33] and GASBOR[34] 20 times individually, followed by superposition and averaging with DAMAVER.[35] The shape of CgNup116(882–1034) was also computed from the merged experimental SAXS profile by SASTBX (http://sastbx.als.lbl.gov/wiki/) and compared with DAMMIF/GASBOR shapes.

RESULTS AND DISCUSSION

Structure of CgNup116(882–1034)

The crystal structure of CgNup116(882–1034) was determined at a resolution of 1.94 Å (Fig. 1(A) and Table I). The monoclinic crystals (space group $P2_1$) contain two molecules per asymmetric unit. Chain A could be traced continuously from Asp882 to Leu1034, whereas in chain B residues 960–963 appear disordered. Otherwise, the A and B chains are essentially identical, with a root-mean-square deviation (r.m.s.d.) of ~0.49 Å for 152 C_α atomic pairs, calculated using the SSM[36] routine as implemented in COOT. The N-terminal segment (residues, 882–893) of CgNup116(882–1034) is well defined

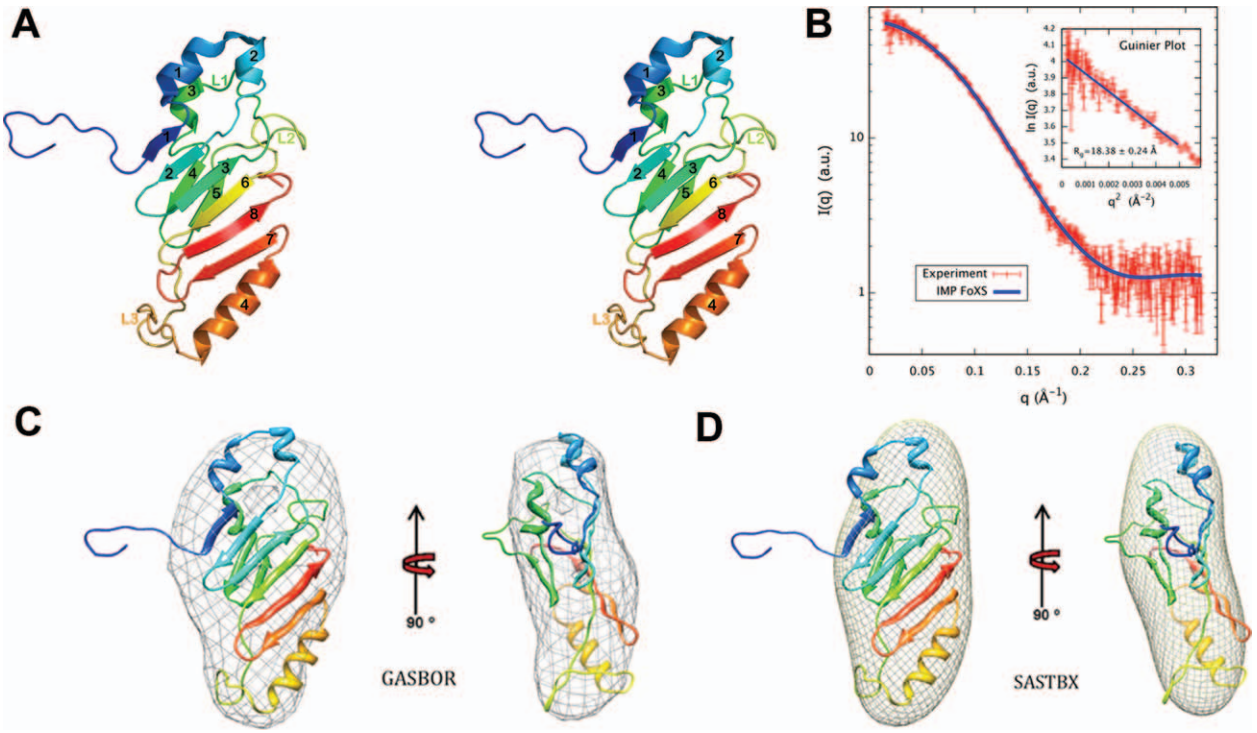

Figure 1

(**A**) Stereoview of the CgNup116(882–1034) monomer. Cartoon of Chain A is shown as a rainbow from blue to red from N- to C-terminus. (**B**) Comparison of the merged experimental SAXS profile (red) of CgNup116(882–1034) with the SAXS profile computed by IMP FoXS (blue) from the complete monomer model of CgNup116(882–1034). Inset shows the SAXS profiles in the Guinier plot, with a R_g fit of 18.38 ± 0.24 Å. D_{max} of radial distribution function, $P(r)$, is 60.65 Å. (**C** and **D**) Comparison of the shapes of CgNup116(882–1034) (represented as a mesh) calculated from the experimental SAXS profile by GASBOR (C) and SASTBX (D).

in the electron density maps and adopts noncanonical secondary structure (i.e., random coil). The overall fold of CgNup116(882–1034) contains two central antiparallel β-sheets flanked by α-helices [Fig. 1(A)]. A six-stranded β-sheet is formed by β1-β2-β3-β6-β8-β7 and a two-stranded β-sheet is formed by β4-β5. Helices α1, α2, and α3 (α3 is a short 3_{10} helix within loop L1) form a cap near the N-terminus and helix α4 caps the six-stranded β-sheet near the C-terminus. CgNup116(882–1034) possesses three long loops including, L1 (residues 930–939 between β3 and β4), L2 (residues 958–974 between β5 and β6), and L3 (residues 980–999 between β6 and α4).

The interface area and the gap volume index[37] between the A and B chains of CgNup116(882–1034), calculated using the NOXclass classifier (http://noxclass.bioinf.mpi-sb.mpg.de/index.php),[38] are ~630 Å^2 and 7.5, respectively. The two copies of CgNup116(882–1034) observed in the crystal asymmetric unit are thus unlikely to represent a physiological dimer, and indeed the merged experimental SAXS profile [Fig. 1(B)] is well matched (χ = 1.11) to the SAXS profile calculated from the complete monomer model of CgNup116(882–1034). The SAXS profile calculated from the complete dimer model resulted in an unacceptably high χ-value of 7.67. The measured radius of gyration (R_g) of 18.38 ± 0.24 Å, determined with AutoRg,[39] is almost identical to the value of 18.1 Å calculated from the complete monomer model of CgNup116(882–1034) (the calculated value of R_g for the A and B chain complex, representing the crystallographic asymmetric unit, is 20.7 Å). Moreover, the "*ab initio*" shape computed from the merged experimental SAXS profile with DAMMIF[33] (data not shown), GASBOR [Fig. 1(C)],[34] and SASTBX [Fig. 1(D)] shows very considerable similarity to our X-ray structure of the CgNup116(882–1034) monomer. Finally, based on the merged experimental SAXS profile, OLIGOMER[40] estimates 100% monomer composition. Thus, our SAXS analyses of the solution behavior of CgNup116(882–1034) and the X-ray crystallographic structure of the monomer are fully consistent with each other.

Comparison of CgNup116(882–1034) with the structures of ScNup116

A pairwise local alignment of CgNup116(882–1034) and ScNup116, computed using LALIGN (http://www.ch.embnet.org/software/LALIGN_form.html), shows sequence identity of 60.1%, whereas sequence identities

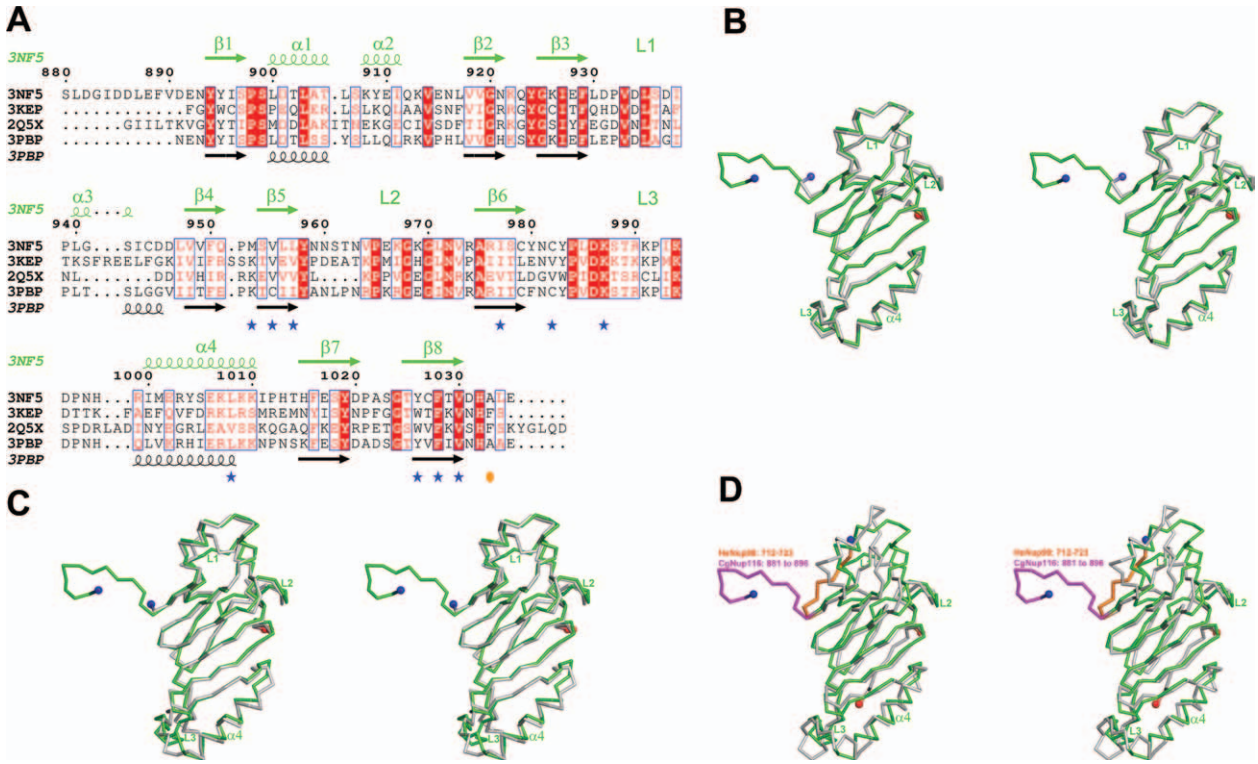

Figure 2

(**A**) Structure-based sequence alignment of the structures of CgNup116(882–1034, PDB Code 3NF5), ScNup116 bound to ScNup82:ScNup159 complex (PDB Code 3PBP), autoproteolytic domain of ScNup145 (PDB Code 3KEP), and autoproteolytic domain of HsNup98 (PDB Code 2Q5X). Secondary structural elements of CgNup116(882–1034) and ScNup116 bound to ScNup82:ScNup159 complex are displayed in green and black, respectively. Residues of ScNup116 contributing to its binary interaction with ScNup82 β-propeller domain[18] are marked with blue star. Sites of autoproteolysis of ScNup145N and HsNup98 are indicated with an orange circle. The Ser residue at the autoproteolytic site of ScNup145N and HsNup98 is replaced by Glu and Ala in proteins used for structure determination, respectively. (**B**) Stereoview of CgNup116(882–1034, green) superposed on the structure of ScNup116 bound to ScNup82:ScNup159 complex (gray). Helix α4 of CgNup116 is structurally equivalent to the helix αB of ScNup116.[18] (**C**) Stereoview of the CgNup116(882–1034, green) superposed on the autoproteolytic domain of ScNup145 (gray). (**D**) Stereoview of the CgNup116(882–1034, green) superposed on the autoproteolytic domain of HsNup98 (gray). Residues preceding the β1-strands are highlighted in magenta and orange for CgNup116(882–1034) and HsNup98, respectively. The N- and C-terminal residues are shown on the cartoons as blue and red spheres, respectively.

of CgNup116(882–1034) drop to 34.5 and 30.6% for the autoproteolytic domains of ScNup145N and HsNup98, respectively. A multiple structural alignment was obtained with the Multiprot[41] (http://bioinfo3d.cs.tau.ac.il/MultiProt/) and STACCATO programs to enable the identification of structurally conserved residues across CgNup116(882–1034), ScNup116 bound to the Nup82–Nup159 complex,[18] ScNup145N,[19] and HsNup98.[11] The alignment demonstrates conservation of the overall fold, despite varying pairwise sequence identities, with an average r.m.s.d. of 1.28 Å over 102 alignment positions with C_α atoms from all four structures. The alignment also reveals positions with a conserved residue type as well as gaps in loop regions [Fig. 2(A)]. The alignment of CgNup116(882–1034) with ScNup116 bound to the Nup82–Nup159 complex suggests that ScNup116 undergoes only a minimal conformational change upon binding to the N-terminal seven-bladed β-propeller domain of Nup82, with only α4-helix (structurally equivalent to helix αB in ScNup116)[18] and loop L3 showing significant structural differences [Fig. 2(B)]. ScNup116 contributes (i) a hydrophobic groove on its surface between the β5-strand and the αB-helix, which forms a binding pocket for the "FGL" motif from the 3D4A loop of ScNup82, and (ii) loop L3, referred to as the "K-loop," situated between the β6-strand and the αB-helix (in particular, the conserved Lys1063 of ScNup116 interacts with Asp204 of ScNup82).[16] In total, 7 out of 10 ScNup116 residues involved in their interaction with ScNup82 are identical in CgNup116 (Fig. 2(A) and Supporting Information Fig. S1). ScNup116 residues Lys1029, Cys1031, and Ile1033 (all from β5-strand) are replaced by Met953, Val955, and Leu957, respectively, at structurally equivalent positions in CgNup116, suggesting possible species specific differences in Nup116:Nup82 interactions.

A structural comparison (data not shown) of CgNup116(882–1034) with the solution NMR structure of ScNup116 (PDB Code 2AIV)[17] also revealed a similar overall structure. The N-terminal α-helices and the β-strands of both central β-sheets are arranged similarly, with the largest difference between the two structures occurring in the L2 loop connecting the β5 and β6 strands. Residues comprising the β5-strand and the N-terminus of the L2 loop have been implicated in the binding of ScNup145C-peptide to ScNup116.[17] In addition, loop L3 and the polypeptide chain segment following α4-helix exhibit significant conformational differences, which is consistent with the conformational flexibility revealed by the solution NMR structures in this region.[17]

Comparison of CgNup116(882–1034) with yeast Nup145 and human Nup98

Both the ScNup145N and the human Nup98 are generated from larger precursors via post-translational autoproteolysis at a conserved Phe-Ser peptide bond[10,11] [Fig. 2(A)]. Nup116, Nup100, and Nup145N are paralogs, and they share an orthologous relationship with human Nup98. CgNup116(882–1034) and ScNup145N's autoproteolytic domain share moderate sequence identity (34.5%). However, overall structures of CgNup116(882–1034) and ScNup145N (PDB Code 3KEP)[19] are virtually identical [Fig. 2(C)]. The only notable conformational difference between these two structures is in loop L1, which includes the 3_{10} helix α3. This difference could result from an insertion within loop L1 in ScNup145N [Fig. 2(A)].

CgNup116(882–1034) is also similar to human Nup98 (PDB Code 2Q5X)[11] [Fig. 2(A,D)]. The main structural differences are the consequence of deletions in loops L1 and L2 as well as an insertion in loop L3. In addition, the structures of CgNup116(882–1034) and human Nup98 differ in the random-coil segment that precedes strand β1 [Fig. 2(D)]. In the human Nup98 autoproteolytic domain, these residues (712–723) fold toward the core. In contrast, the equivalent residues (882–893) of CgNup116(882–1034) project away from the core [Fig. 2(D)]. Moreover, the conformational plasticity of residues 882–893 in CgNup116(882–1034) is revealed by the absence of any features corresponding to these residues in the solution shapes computed from the SAXS profiles [Fig. 1(C,D)] of CgNup116(882–1034). These results suggest that the residues preceding the β1 strand may adopt different conformations in the NPC targeting domain of CgNup116 and the autoproteolytic domain of human Nup98.

Protein Data Bank Codes

Atomic co-ordinates and structure factors of CgNup116(882–1034) were deposited to the PDB on 09 June 2010 with accession codes 3NF5. The NYSGXRC target identifier for CgNup116 in TargetDB (http://targetdb.pdb.org) is "NYSGXRC-15100c." Expression clone sequences and selected interim experimental results are available in PepcDB (http://pepcdb.pdb.org/).

ACKNOWLEDGMENTS

The authors thank members of the NYSGRC, Rout, and Sali laboratories for their help and advice. Use of the Advanced Photon Source was supported by the U.S. Department of Energy, Office of Basic Energy Sciences. Access to the LRL-CAT beam line facilities at Sector 31 of the APS was provided by Eli Lilly, which operates the facility. Portions of this research were carried out at the Stanford Synchrotron Radiation Lightsource, a Directorate of SLAC National Accelerator Laboratory and an Office of Science User Facility operated for the US Department of Energy Office of Science by Stanford University. The contents of this publication are solely the responsibility of the authors and do not necessarily represent the official view of NCRR or NIH.

REFERENCES

1. Xu S, Powers MA. Nuclear pore proteins and cancer. Semin Cell Dev Biol 2009;20:620–630.
2. Cronshaw JM, Matunis JM. The nuclear pore complex: disease associations and functional correlations. Trends Endocrinol Met 2004;15:34–39.
3. Rout MP, Aitchison JD, Suprapto A, Hjertaas K, Zhao YM, Chait BT. The yeast nuclear pore complex: composition, architecture, and transport mechanism. J Cell Biol 2000;148:635–651.
4. D'Angelo MA, Hetzer MW. Structure, dynamics and function of nuclear pore complexes. Trends Cell Biol 2008;18:456–466.
5. Alber F, Dokudovskaya S, Veenhoff LM, Zhang WH, Kipper J, Devos D, Suprapto A, Karni-Schmidt O, Williams R, Chait BT, Sali A, Rout MP. The molecular architecture of the nuclear pore complex. Nature 2007;450:695–701.
6. Alber F, Dokudovskaya S, Veenhoff LM, Zhang WZ, Kipper J, Devos D, Suprapto A, Karni-Schmidt O, Williams R, Chait BT, Rout MP, Sali A. Determining the architectures of macromolecular assemblies Nature 2007;450:683–694.
7. Wente SR, Rout MP, Bobel G. A new family of yeast nuclear pore complex proteins J Cell Biol 1992;119:705–723.
8. Strawn L, Shen T, Wente SR. The GLFG regions of Nup116p and Nup100p serve as binding sites of both Kap95p and Mex67p at the nuclear pore complex. J Biol Chem 2001;276:6445–6452.
9. Ho AK, Shen T, Ryan KJ, Kiseleva E, Levy MA, Allen TD, Wente SR. Assembly and preferential localization of Nup116p on the cytoplasmic face of the nuclear pore complex by interaction with Nup82p. Mol Cell Biol 2000;20:5736–5748.
10. Hodel EA, Hodel MR, Griffis ER, Hennig KA, Ratner GA, Xu S, Powers MA. The three-dimensional structure of the autoproteolytic, nuclear pore-targeting domain of the human nucleoporin Nup98. Mol Cell 2002;10:347–358.
11. Sun Y, Guo H.-C. Structural constraints on autoprocessing of the human nucleoporin Nup98. Protein Sci 2008;17:494–505.
12. Bailer SM, Balduf C, Katahira J, Podtelejnikov A, Rollenhangen C, Mann M, Pante N, Hurt E. Nup116p associates with the Nup82p-Nsp1p-Nup159p nucleoporin complex J Biol Chem 2000;275:23540–23548.

13. Suntharalingam M, Wente SR. Peering through the pore: nuclear pore complex structure, assembly, and function. Dev Cell 2003;4: 775–789.
14. Bailer S M, Siniossoglou S, Podtelejnikov A, Hellwig A, Mann M, Hurt E. Nup116p and nup100p are interchangeable through a conserved motif which constitutes a docking site for the mRNA transport factor gle2p. EMBO J 1998;17:1107–1119.
15. Blevin MB, Smith AM, Phillips EM, Powers MA. Complex formation among the RNA export proteins Nup98, Rae1/Gle2 and TAP. J Biol Chem 2003;278:20979–20988.
16. Ren Y, Seo H-S, Blobel G, Hoelz A. Structural and functional analysis of the interaction between the nucleoporin Nup98 and the mRNA export factor Rae1 Proc Natl Acad Sci 2010;107:10406–10411.
17. Robinson MA, Park S, Sun ZJ, Silver PA, Wagner G, Hogle JM. Multiple conformations in the ligand-binding site of yeast nuclear pore-targeting domain of Nup116p. J Biol Chem 2005;280: 35723–35732.
18. Yoshida K, Seo H-S, Debler EW, Blobel G, Hoelz A. Structural and functional analysis of an essential nucleoporin heterotrimer on the cytoplasmic face of the nuclear pore complex. Proc Natl Aca Sci USA 2011;108:16571–16576.
19. Sampathkumar P, Ozyurt SA, Do J, Bain KT, Dickey M, Rodgers LA, Gheyi T, Sali A, Kim SJ, Phillips J, Pieper U, Fernandez-Martinez J, Franke JD, Martel A, Tsuruta H, Atwell S, Thompson DA, Emtage JS, Wasserman SR, Rout MP, Sauder MJ, Burley SK. Structure of the autoproteolytic domain from the *Saccharomyces cerevisiae* nuclear pore complex component, Nup145. Proteins Struct Funct Bioinformatics 2010;78:1992–1998.
20. Van Duyne GD, Standaert RF, Karplus PA, Schreiber SL, Clardy J. Atomic structures of human immunophilin FKBP-12 complexes with FK506 and Rapamycin. J Mol Biol 1993;229:105–124.
21. Leslie AGW, Brick P, Wonacott AJ. An improved program package for the measurement of oscillation photographs. CCP4 News 1986;18:33–39.
22. Collaborative Computing Project Number 4. The CCP4 suite: programs for protein crystallography. Acta Crystallogr D Biol Crystallogr 1994;50:760–763.
23. McCoy A J, Grosse-Kunstleve RW, Adams PD, Winn MD, Storoni LC, Read RJ. PHASER crystallographic software. J Appl Crystallogr 2007;40:658–674.
24. Perrakis A, Morris R, Lamzin VS. Automated protein model building combined with iterative structure refinement. Nat Struct Biol 1999;6:458–463.
25. Emsley P, Cowtan K. COOT: model-building tools for molecular graphics. Acta Crystallogr D Biol Crystallogr 2004;60:2126–2132.
26. Murshudov GN, Vagin AA, Dodson EJ. Refinement of macromolecular structures by the Maximum-Likelihood Method. Acta Crystallogr D Biol Crystallogr 1997;53:240–255.
27. DeLano WL. The PyMOL Molecular Graphics System. 2002; Availabale at: http://pymol.sourceforge.net.
28. Blu-Ice and the Distributed Control System: software for data acquisition and instrument control at macromolecular crystallography beamlines.McPhillips TM, McPhillips SE, Chiu HJ, Cohen AE, Deacon AM, Ellis PJ, Garman E, Gonzalez A, Sauter NK, Phizackerly RP. J Synchrotron Radiat 2002;9:401–406.
29. Forster F, Webb B, Krukenberg KA, Tsuruta H, Agard DA, Sali A. Integration of small-angle X-ray scattering data into structural modeling of proteins and their assemblies. J Mol Biol 2008;382: 1089–1106.
30. Schneidman-Duhovny D, Hammel M, Sali A. FoXS: a web server for rapid computation and fitting of SAXS profiles (Web Server Issue). Nucleic Acids Res 2010;38:W540–W544.
31. Sali A, Blundell TL. Comparative protein modelling by satisfaction of spatial restraints. J Mol Biol 1993;234:779–815.
32. Russel D, Lasker K, Webb B, Velazquez-Muriel J, Tjioe E, Schneidman-Duhovny D, Peterson B, Sali A. Putting the pieces together: integrative structure determination of macromolecular assemblies. PLoS Biol 10(1), e1001244. DOI:10.1371/journal.pbio. 1001244.
33. Franke D, Svergun DI. DAMMIF, a program for rapid *ab-initio* shape determination in small-angle scattering. J Appl Cryst 2009;42:342–346.
34. Svergun DI, Petoukhov MV, Koch MHJ. Determination of domain structure of proteins from X-ray solution scattering. Biophys J 2001;80:2946–2953.
35. Volkov VV, Svergun DI. Uniqueness of *ab initio* shape determination in small-angle scattering. J Appl Cryst 2003;36:860–864.
36. Krissinel E, Henrick K. Secondary-structure matching (SSM), a new tool for fast protein structure alignment in three dimensions. Acta Crystallogr D Biol Crystallogr 2004;60:2256–2268.
37. Bahadur R, Chakrabarti P, Rodier F, Janin J. A dissection of specific and non-specific protein-protein interfaces. J Mol Biol 2004;336: 943–955.
38. Zhu H, Domingues FS, Sommer I, Lengauer T. NOXclass: prediction of protein-protein interaction types. Biomed Chromatogr Bioinformatics 2006;7:27 (Available at: http://noxclass.bioinf.mpi-sb.mpg.de/index.php).
39. Konarev PV, Kikhney AG, Franke D, Petoukhov MV, Svergun DI. Automated SAXS Data Processing on the X33 Beamline. HASY LAB Annual Report 2007;Part II:339–340.
40. Konarev PV, Volkov VV, Sokolova AV, Koch MHJ, Svergun DI. PRIMUS: a Windows PC-based system for small-angle scattering data analysis. J Appl Cryst 2003;36:1277–1282.
41. Shatsky M, Nussinov R, Wolfson HJ. A method for simultaneous alignment of multiple protein structures. PROTIENS: Struct Funct Bioinformatics 2004;56:143–156.
42. Ramakrishnan C, Ramachandran GN. Stereochemical criteria for polypeptide and protein chain conformations. II. Allowed conformations for a pair of peptide units. Biophys J 1965;5:909–933.
43. Davis IW, Leaver-Fay A, Chen VB, Block JN, Kapral GJ, Wang X, Murray L.W, Arendall III WB, Snoeyink J, Richardson JS, Richardson DC. MolProbity: all-atom contacts and structure validation for proteins and nucleic acids. Nucleic Acids Res 2007;35:W375–W383 (Available at: http://molprobity.biochem.duke.edu/).